

Mechanically-Motivated Selection of Patching Material for the Patient-Specific Carotid Artery

A.V. Kamenskiy¹, I.V. Kirillova², L.Y. Kossovich²
Y.E. Salkovskiy² and Y.A. Dzenis¹

¹University Of Nebraska-Lincoln, Lincoln NE, United States of America

²Saratov State University, Saratov, Russia

Abstract

Patch angioplasty is the most common technique used for performing a carotid endarterectomy. A large number of materials are available for use as patches, but little is known to aid the surgeon in selecting a patch while caring for a patient with carotid disease. The objective of the study, described in this paper, was to suggest a hemodynamically motivated choice of a patch material from those currently used by vascular surgeons. A patient-specific mathematical model of the carotid artery repaired with patch angioplasty was built and used to study atherogenesis-related mechanical factors such as wall shear stress, cyclic strain and effective stress. Model incorporated fluid-structure interaction and non-linear mechanical properties of the arterial wall. The analysis performed indicated that patches made of bovine pericardium may promote better hemodynamics than patches made of synthetic polytetrafluoroethylene and Dacron in terms of reducing stresses and strains in the repaired arterial wall. Our data can aid vascular surgeons in their selection of repair technique for the care of patients undergoing patch angioplasty.

Keywords: carotid artery, patch angioplasty, endarterectomy, bovine pericardium, polytetrafluoroethylene, Dacron.

1 Introduction

Atherosclerosis of the carotid artery bifurcation is a leading cause of stroke. Endarterectomy has been shown to significantly reduce the risk of stroke in patients with severe carotid bifurcation stenosis [1, 2, 3]. The standard approach for the performance of endarterectomy involves a longitudinal arteriotomy from the common (CCA) to the internal carotid artery (ICA) followed by removal of the atherosclerotic plaque. There is significant clinical evidence that closing the longitudinal arteriotomy after endarterectomy using a patch is superior to common

primary closure in reducing the risk of restenosis and improving both short and long term clinical outcomes [4, 5, 6, 7, 8, 9]. As a result, a large variety of materials have been made available for use as patches. These include synthetic polytetrafluoroethylene and Dacron, and biological bovine pericardium and autologous vein. All these materials (except vein) are commercially available; however, there is currently minimal data to aid the surgeon in choosing a patch while caring for a patient with carotid disease [10]. The study of the biomechanical behavior and hemodynamic properties of the patched carotid artery may help to define the patch of choice among those currently available. Such study is best performed with the help of mathematical modeling.

In recent years mathematical modeling of arteries has matured immensely with the emergence of better imaging, modeling, mesh generation, computation, and visualization technologies. State-of-the-art models incorporate fully coupled fluid-structure interaction, and account for substantial arterial wall non-linearity. Such simulations are done in an effort to investigate certain hemodynamic factors that influence the onset and progression of cardiovascular disease. In this context special attention has been given to models of healthy [11, 12] and severely diseased arteries [13, 14, 15], yet surprisingly little consideration was given to studies of the endarterectomized and patched carotids [10].

The goal of the present work was to investigate the biomechanics of the endarterectomized and patched carotid artery, and to find the optimal patching material among those commonly used by the surgeons of the Bakoulev Scientific Center for Cardiovascular Surgery. Developed mathematical model is based on the three-dimensional patient-specific geometry and experimentally determined mechanical properties. It incorporates *in vivo* measured flow boundary conditions, and accounts for mutual interaction between the arterial wall and the blood flow. Selection of the patch material is based on analysis of wall shear stress, cyclic strain and effective stress as these mechanical factors are believed to be associated with atherogenesis [16, 17, 18, 19, 20, 21].

2 Methods

2.1 Evaluation of the Mechanical Properties of Carotid Arteries and Patch Materials

A total of eight (N=8) human cadaveric carotid specimens were harvested from patients that had no prior carotid operations. Use of autopsy material from human subjects was approved by the Ethics Committee of the Saratov State Medical University. All institutional policies were followed during data collection and analysis.

Common carotid segments just proximal to the cervical bifurcation were harvested within six hours from the time of death and were tested immediately after harvesting. Tissues obtained using such rapid autopsy techniques were shown to maintain the *in vivo* mechanical properties [22, 23, 24]. Testing was performed using a TiraTest 28005 Uniaxial tensile evaluation device (Tira, WPM Leipzig, Germany). The stress-stretch curves for the principal direction and the concurrent change in width of the material were measured while the change in the material thickness was calculated from the two measured dimensions assuming tissue incompressibility [25]. Experimental stress-strain curves for all tested carotids were computed after 10 cycles of preconditioning of the material.

Mechanical properties of six different types of commercially available patches (4 types of polytetrafluoroethylene by Ecoflon, Dacron patch by UMK Technology and chemically treated bovine pericardium by Bakoulev Scientific Center for Cardiovascular Surgery) were evaluated using the same testing protocols. Data on tested patch materials are summarized in Table 1. We did not include autologous vein patches in our study, because vein may frequently be unavailable due to prior harvesting or vein disease.

#	Patch Type	Material	Thickness, mm	Density, g/cm ³	a , kPa	b
1	Ecoflon PS 442 93 0101	Polytetrafluoroethylene	0.4	0.598	3880	51
2	Ecoflon PS 433 15 0101	Polytetrafluoroethylene	0.4	0.369	3750	76
3	Ecoflon PS 442 19 0107	Polytetrafluoroethylene	0.6	0.355	3750	76
4	Ecoflon PS 442 94 0101	Polytetrafluoroethylene	0.6	0.630	4750	86
5	UMK Tech M002020195790	Dacron	0.38	0.508	3380	45
6	BSCCS bovine pericardium	Bovine pericardium	0.45	1.6179	74	23

Table 1. Types of patch materials used in the study, and constitutive model parameters a and b that describe material properties

2.2 Mathematical model

Results of Computerized Tomographic Imaging of a 67 y.o. patient with severe (>80%) carotid bifurcation stenosis were used for reconstruction of the three-dimensional carotid artery geometry. A 12-cm segment of the artery was built by segmenting the cross-sections of the tomogram and connecting them into the three-dimensional model in Computer Aided Design Software [10]. Changes in radiodensity were used to determine the wall thickness and borders of the atherosclerotic plaque. Patch was introduced to the model by removing part of the arterial wall and substituting it with a patch of given thickness.

Coupled fluid-structure boundary value problem was set up through separate mathematical descriptions in each of the fluid and solid domains. To account for the movement of the fluid mesh at the boundary with the solid domain, we have used Arbitrary Lagrangian-Eulerian formulation for the conservation of mass and momentum equations for the fluid. This was achieved by replacing the material velocity \mathbf{u} which appears in the convective term of Eulerian formulations with a convective velocity $(\mathbf{u} - \mathbf{u}_g)$:

$$\nabla \cdot \mathbf{u} = 0 \quad (1)$$

$$\rho_f \left(\frac{\partial \mathbf{u}}{\partial t} + ((\mathbf{u} - \mathbf{u}_g) \cdot \nabla) \mathbf{u} \right) = -\nabla p_f + \nabla \cdot \boldsymbol{\tau} \quad (2)$$

here ρ_f is fluid density, p_f is pressure, \mathbf{u} is the fluid velocity vector and \mathbf{u}_g is the moving coordinate velocity (mesh velocity), so $(\mathbf{u} - \mathbf{u}_g)$ is the relative velocity of the fluid with respect to the moving coordinate velocity. Further, $\boldsymbol{\tau}$ is the deviatoric stress tensor, related to strain rate tensor $\dot{\boldsymbol{\gamma}}$ as

$$\boldsymbol{\tau} = \mu \dot{\boldsymbol{\gamma}} \quad (3)$$

where μ is fluid viscosity that was assumed constant [12, 26, 14, 27] and was taken as 0.004 Pa·s [10]. Density of the blood was set to 1100 kg/m³ [10].

Momentum conservation equation in the Lagrangian description with large displacements and large strains was solved for the solid domain:

$$\nabla \cdot \boldsymbol{\sigma}_s = \rho_s \ddot{\mathbf{d}}_s \quad (4)$$

where ρ_s is density of the solid, $\boldsymbol{\sigma}_s$ is the solid stress tensor, and $\ddot{\mathbf{d}}_s$ is the local acceleration of the solid. Arterial wall was assumed to be homogeneous, incompressible, hyperelastic material with a density $\rho_s = 1050 \text{ kg/m}^3$.

Constitutive law for the arterial wall and patch was selected out of several possibilities in the form proposed by Delfino [28]. Strain energy function W is then:

$$W = \frac{a}{b} \left(\exp\left(\frac{b}{2} (\mathbf{I}_1 - 3)\right) - 1 \right) \quad (5)$$

where a, b are material parameters and \mathbf{I}_1 is the first invariant of the Cauchy-Green deformation tensor. Cauchy stress tensor $\boldsymbol{\sigma}_s$ can then be calculated from (6) as (assuming incompressibility):

$$\boldsymbol{\sigma}_s = \mathbf{F} \frac{\partial W}{\partial \mathbf{F}} - p \mathbf{I} = \alpha_1 \mathbf{B} + \alpha_2 \mathbf{B}^2 - p \mathbf{I} \quad (6)$$

where \mathbf{F} is the deformation gradient tensor, \mathbf{B} is the left Cauchy-Green deformation tensor, p is Lagrange multiplier associated with the incompressibility constraint

$\det \mathbf{F} = 1$, and $\alpha_1 = 2\left(\frac{\partial w}{\partial \mathbf{I}_1} + \mathbf{I}_1 \frac{\partial w}{\partial \mathbf{I}_2}\right)$, $\alpha_2 = -2\frac{\partial w}{\partial \mathbf{I}_2}$, where \mathbf{I}_1 and \mathbf{I}_2 are invariants of \mathbf{B} .

Material parameters a and b were found by fitting equations (6) to the uniaxial tensile experimental data, and subsequent minimization procedure using Levenberg-Marquardt algorithm.

Motion of the fluid boundary along with the solid wall, conservation of mass, momentum and mechanical energy on the interface were fulfilled by imposing the kinematic and dynamic conditions on the interface. Those included compatibility of displacements of the fluid and solid domains, equilibrium of tractions on the interface, and no-slip conditions for the blood flow. Coupling was achieved through passing fluid stress at the boundary to the structural solver as an applied load. After finding the structural solution, the structural solver returned the resulting boundary displacements to the fluid solver, providing the latter with updated flow geometry. Flow geometry was updated through transfinite interpolation and nodal constraints. The iterative process continued at each time step until solutions at the boundary were sufficiently compatible [29].

2.3 Boundary conditions

Boundary conditions for the model contained post-operatively measured blood pressure and velocity. Blood pressure was determined as 120/70 mm Hg using non-invasive auscultatory cuff measurements. We assumed that these values were similar to the actual pressure in the common carotid artery (CCA). Velocity was measured in the center lumen of the internal (ICA) and external (ECA) carotid arteries sufficiently far off the bifurcation using Duplex Ultrasound. ICA velocities were determined as 150 and 37 cm/s for peak systole and end diastole respectively. ECA velocities were measured as 110 and 20 cm/s. We assumed that the velocity profiles in the carotid were axisymmetric about the arterial centerline when measured far off the bulb. We then followed the methodology reported by Younis et al [12] in generating Womersley-type profiles describing spatial distribution of velocity throughout the lumen. Since the ICA and ECA cross-sections were nearly circular, flow velocities were generated using the equivalent radii of these cross-sections (the equivalent radius is the radius of a circle with the same area as the cross-section). The resulting axisymmetric profiles predicted the velocity distribution as a function of radial position from the center of the equivalent circular vessel. Generated velocity profiles were then applied to the nodes on the outlet planes of the ICA and ECA as time-dependent functions.

3 Results

3.1 Mechanical Properties of Carotid Arteries and Patch Materials

Stress-stretch curves for the tested carotid arteries are presented in Figure 1 a). All arteries demonstrated appreciable variability, and exponent-like behavior conditioned by the undulated collagen fibers inside the tissue. Specimen #3 appeared to have “average” properties of all tested specimens. Because of that, its properties were chosen for subsequent modeling. Constitutive model parameters of (5) for this specimen were found to be $a = 48.52$ kPa and $b = 18.42$ ($R = 0.99$).

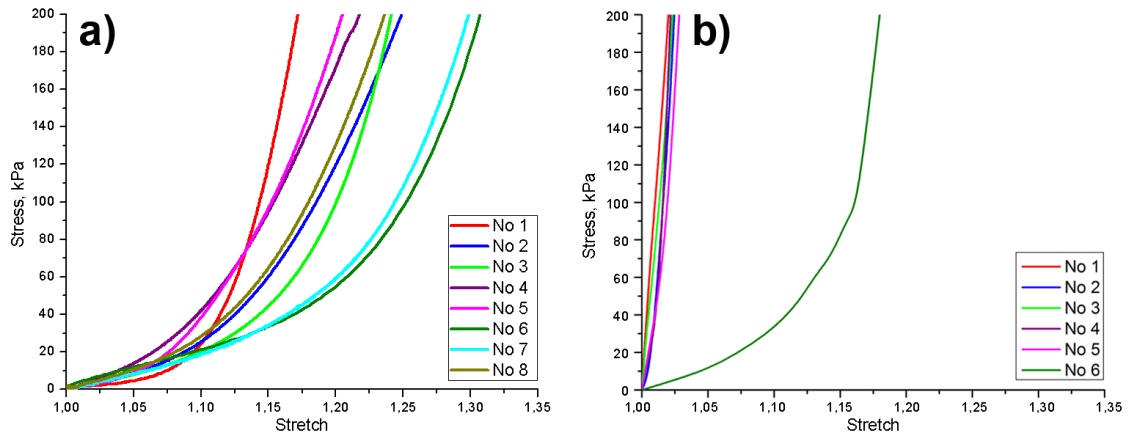


Figure 1. Experimental stress-stretch relations for (a) human carotid arteries, and (b) patch materials

Stress-stretch curves for the patch materials are presented in Figure 1 b). Synthetic patches (polytetrafluoroethylene and Dacron, #1-5) have demonstrated linear elastic response and substantially higher stiffness compared to carotid tissue. Bovine pericardium patch (#6) on the other hand showed the exponent-like behavior similar to the one of the carotid arteries. Constitutive model parameters of (5) determined for all patches are summarized in Table 1.

3.2 Mathematical Modeling

Wall Shear Stress (WSS) distributions at peak systole for arteries repaired with all six patch materials are presented in Figure 2. Common logarithm of WSS was calculated to emphasize the low-value zones, in which WSS is thought to be atherogenic [17]. WSS was calculated by multiplying dynamic viscosity with the velocity gradient in the direction of local unit surface normal \hat{n}_s :

$$\tau_s = \mu \frac{\partial \mathbf{u}}{\partial \hat{n}_s} \quad (7)$$

here τ_s is the WSS, μ is blood viscosity and $\frac{\partial \mathbf{u}}{\partial \hat{\mathbf{n}}_s}$ is the velocity gradient in the direction of surface normal.

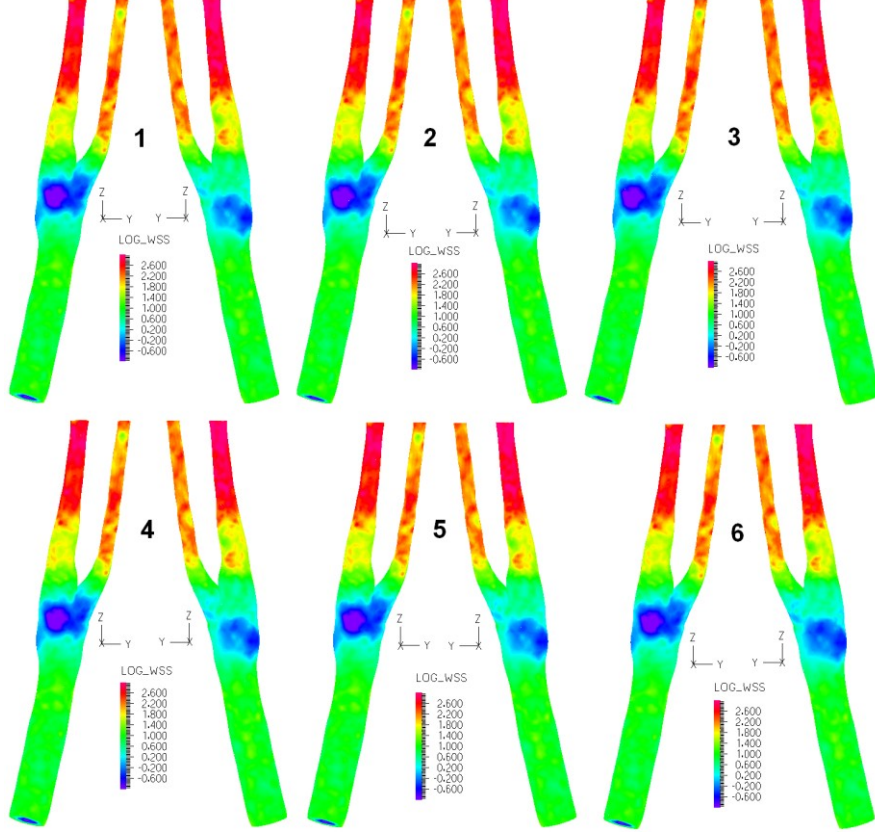


Figure 2. Common logarithm of Wall Shear Stress at peak systole. Carotid wall and patch are removed from the figure for better visualization. Numbers indicate patch type according to Table 1

All six WSS distributions were very similar, which indicates that patch material has a minor influence on the arterial WSS. Low WSS was concentrated in the carotid bulb, with lowest values observed posteriorly and proximally to the flow divider. Location of the lowest WSS on the posterior side indicates that angioplasty stiffened the artery anteriorly and resulted in bulging of the opposite posterior wall. Distal ICA and ECA possessed high WSS, which is believed to be atheroprotective [17].

Cyclic Strain (CS) distributions are presented in Figure 3. CS quantifies the amount of arterial wall deformation during the cardiac cycle; therefore it was computed as the difference between Von Mises strains [30] calculated at peak systole and late diastole:

$$\epsilon_{VM,cyclic} = \epsilon_{VM,peak\ systole} - \epsilon_{VM,late\ diastole} \quad (8)$$

where the Von Mises strain is a strain invariant defined by:

$$\epsilon_{VM} = \left[\frac{(\epsilon_I - \epsilon_{II})^2 + (\epsilon_{II} - \epsilon_{III})^2 + (\epsilon_I - \epsilon_{III})^2}{2} \right]^{1/2} \quad (9)$$

and ϵ_I , ϵ_{II} and ϵ_{III} are the logarithmic values of the principal Green strains.

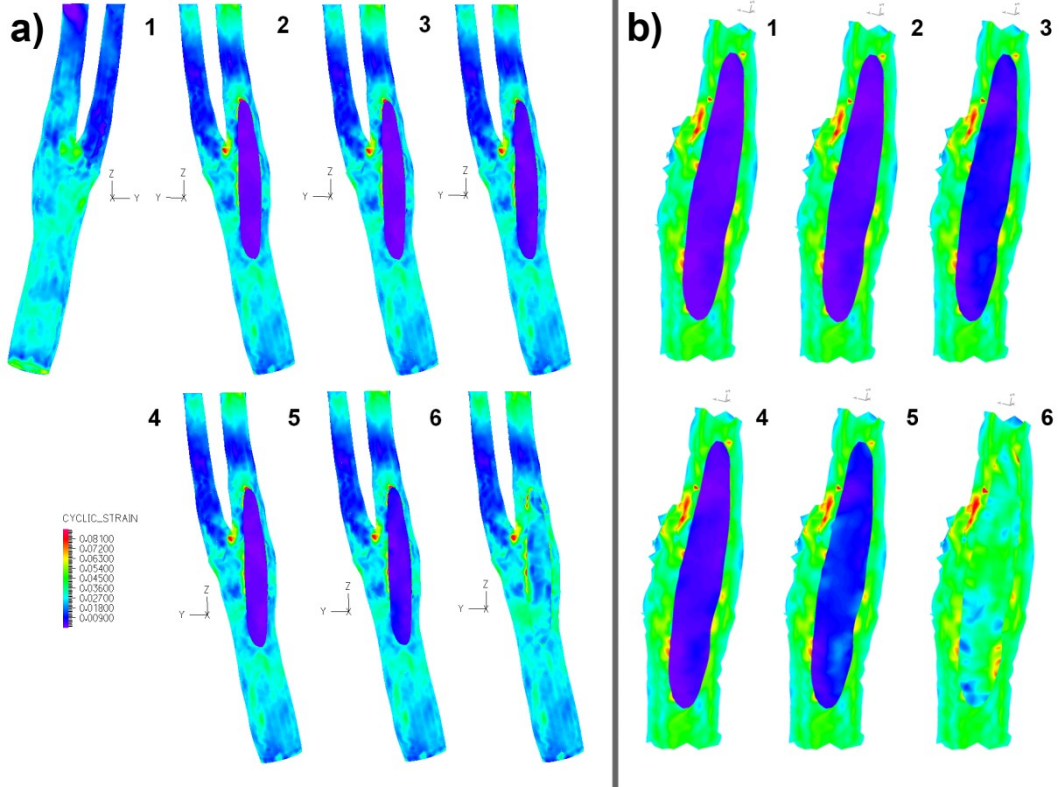


Figure 3. Cyclic Strain distributions for carotid artery repaired with six different types of patch materials (see Table 1): a) anterior and posterior views of the artery, b) magnified view of the angioplasty site viewed from the inside of the artery

CS distributions on the posterior side of the artery were very similar for all six patch materials, therefore only one side is presented in Figure 3 a). Detailed view of the angioplasty site is given in Figure 3 b) with magnified images depicting the inner side of the artery closer to the blood flow. CS of the stiff synthetic patches was close to zero, which indicates that these patches did not deform during the cardiac cycle. In case of bovine patch, CS transitions smoothly from the patch to the arterial wall, indicating better hemodynamics. Locally high CS was observed in the apex and around the patch borders, with higher values occurring on the inner side of the artery, closer to the blood flow.

Effective Stress (ES, Von Mises stress) distributions are plotted in Figure 4. ES was calculated using (9) and substituting principal logarithmic strains with principal stresses. It therefore represents the gross stress response of the artery, which was largest during peak systole.

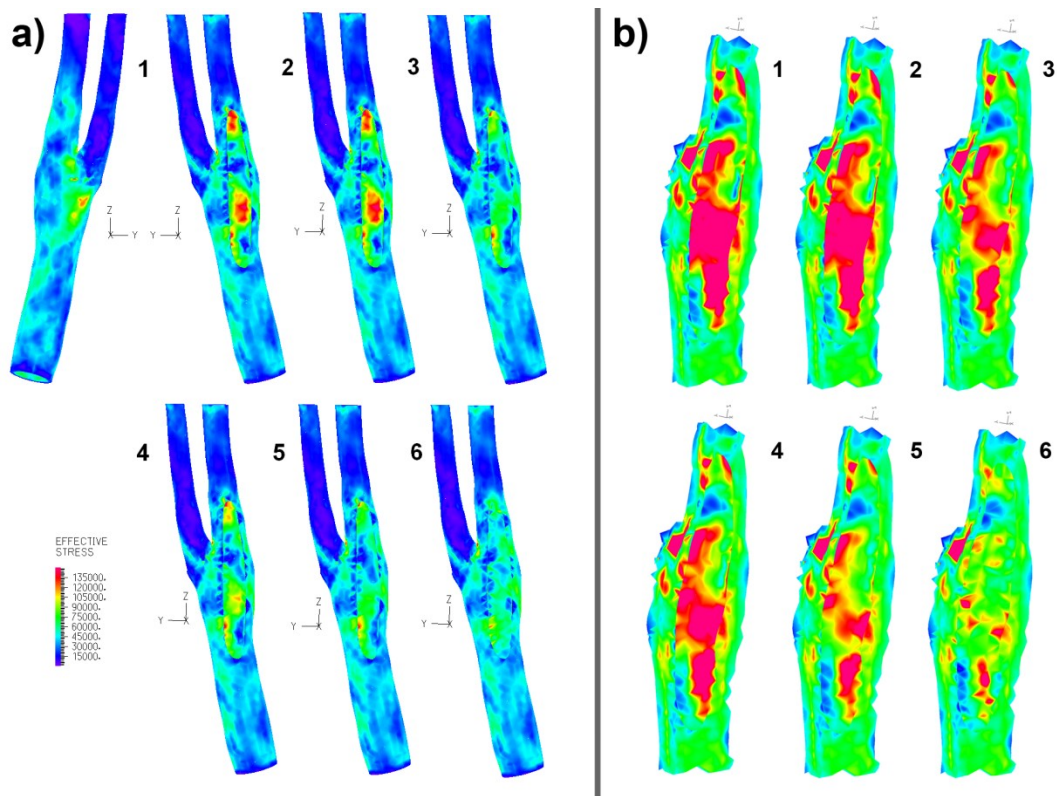


Figure 4. Effective Stress distributions for carotid artery repaired with six different types of patch materials (see Table 1): a) anterior and posterior views of the artery, b) magnified view of the angioplasty site viewed from the inside of the artery. Distributions are presented for peak systole

High ES was observed diffusely in the carotid bulb for all six arterial repairs. Particularly high ES was localized around the patch borders, on the patch surface, in the carotid apex and at the takeoff of the ECA. Higher ES was observed on the inner surface of the artery, closer to the blood flow. For synthetic patches values of ES were higher than for bovine pericardium. Latter showed smooth transition of stresses from the patch to the host arterial wall.

Unlike WSS and CS, ES metric provided better visual information for patch comparison, clearly showing the differences in stress concentrations. In order to study these differences in greater detail, we have identified six zones of locally high ES seen in Figure 4 b). These locations were selected around the patch with zones 1 and 5 located laterally; zones 2 and 3 located medially; zone 4 - proximally; and zone 6 - distally. Values of ES for all six zones are presented in Figure 5.

Values of ES for bovine pericardium were on average 1.8-fold smaller than those for polytetrafluoroethylene patches. Largest difference was observed laterally, while smallest difference was seen distally. Dacron patch showed lower ES than polytetrafluoroethylene, but on average 1.3-fold larger ES than bovine pericardium.

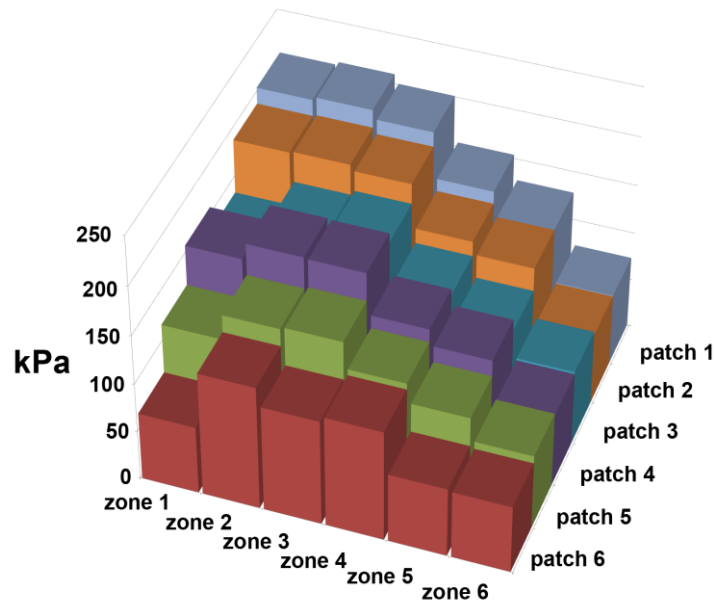


Figure 5. Comparison of ES (kPa) in six zones of locally high values for six types of patch materials

4 Discussion

With the help of mathematical modeling, we were able to study the hemodynamics of the endarterectomized and patched carotid artery, and to successfully calculate wall shear stress, cyclic strain and effective stress for arteries repaired with different patch materials. Wall shear stress, cyclic strain and effective stress have been implicated in the pathogenesis of atherosclerosis and neointimal hyperplasia [16, 17, 18, 12, 19, 20, 21].

The hemodynamic mechanism of atherogenesis that links low wall shear stress to disease was initially postulated by Fry [31] and Caro et al [16]. They noticed that the natural widening of the carotid bulb and the branching into the internal and external carotids perturb the normal laminar flow present in the more proximal common carotid artery. Flow alterations occur in both the longitudinal and transverse directions, resulting in boundary layer separation and secondary flow. Both boundary layer separation and secondary flow result in low and oscillatory wall shear stress and higher time of platelet residence. This in turn increases the permeability of the endothelium by ceasing production of Nitric Oxide [32], and also the proteins that form the junctions between the endothelial cells [33]. This may lead to adhesion of monocytes to the endothelium, and development of the atherosclerotic plaque [17].

Our results demonstrate that in the patched carotid, a zone of low wall shear stress can be identified in the bulb with the lowest values occurring at the side opposite to

the patch. This might be due to stiffening of the angioplasty site which may cause the carotid to bulge out opposite to the patch creating a low wall shear stress region. Interestingly, patch material did not have major effect on the flow patterns, and higher compliance of the bovine pericardium did not significantly affect the wall shear stress distribution.

High cyclic strain and effective stress may also be involved in pathogenesis, yet though a different mechanism – arterial wall injury. This mechanism was first described by Ross [34] and Clowes et al [20] who hypothesized that damage of the arterial wall can lead to cell migratory and proliferative responses. Following platelet deposition this may result in slow accumulation of lipoproteins and development of arterial disease [35].

Comparison of arteries repaired with different patch materials showed that all patches produced significant stress and strain concentrations throughout the repaired bifurcation. These locations were registered diffusely in the carotid bulb, in the flow divider, in the patch, around the patch borders and in the adjacent external carotid artery wall. Localization of these zones was the same for all considered patch materials, but values of cyclic strain and effective stress were significantly lower for bovine pericardium than for the synthetic patches. Finding of localized stress and strain concentrations in the bulb and around the patch is consistent with the work of Rosenthal [36] demonstrating higher incidence of post endarterectomy stenosis at the level of the endarterectomized bulb.

There is a considerable debate over the choice of patch material to use for the performance of carotid endarterectomy. Our current work presents the initial effort to determine the best patch material from those currently available. Obtained results encourage for the use of bovine pericardium patches versus synthetic polytetrafluoroethylene or Dacron for reduction of stresses and strains in the repaired arterial wall. Existing evidence in the clinical literature supports this conclusion by demonstrating lower post-surgical complications including the number of transient ischemic attacks and strokes in patients with bovine patches [37]. More targeted medical trials are however required to establish the veracity of this conclusion. In addition, we envision the influence of patch size, geometry and location on arterial stress-strain state. Such studies are currently underway.

References

- [1] A. C. of Cardiology Foundation, A. S. of Interventional & Therapeutic Neuroradiology, S. for Cardiovascular Angiography, Interventions, S. for Vascular Medicine, Biology, S. of Interventional Radiology, E. R. Bates, J. D. Babb, D. E. Casey, C. U. Cates, G. R. Duckwiler, T. E. Feldman, W. A. Gray, K. Ouriel, E. D. Peterson, K. Rosenfield, J. H. Rundback, R. D. Safian, M. A. Sloan, and C. J. White, “Accf/scai/svmb/sir/asitn 2007 clinical expert consensus document on carotid

- stenting: a report of the american college of cardiology foundation task force on clinical expert consensus documents (accf/scai/svmb/sir/asitn clinical expert consensus document committee on carotid stenting).,” *J Am Coll Cardiol*, vol. 49, pp. 126–170, Jan 2007.
- [2] J. J. Ricotta and M. Piazza, “Carotid endarterectomy or carotid artery stenting? matching the patient to the intervention.,” *Perspect Vasc Surg Endovasc Ther*, vol. 22, pp. 124–136, Jun 2010.
- [3] A. Muto, T. Nishibe, H. Dardik, and A. Dardik, “Patches for carotid artery endarterectomy: current materials and prospects.,” *J Vasc Surg*, vol. 50, pp. 206–213, Jul 2009.
- [4] I. A. Awad and J. R. Little, “Patch angioplasty in carotid endarterectomy. advantages, concerns, and controversies.,” *Stroke*, vol. 20, pp. 417–422, Mar 1989.
- [5] A. F. AbuRahma, P. A. Robinson, S. Saiedy, J. H. Kahn, and J. P. Boland, “Prospective randomized trial of carotid endarterectomy with primary closure and patch angioplasty with saphenous vein, jugular vein, and polytetrafluoroethylene: long-term follow-up.,” *J Vasc Surg*, vol. 27, pp. 222–32; discussion 233–4, Feb 1998.
- [6] J. A. D. Letter, F. L. Moll, R. J. Welten, B. C. Eikelboom, R. G. Ackerstaff, F. E. Vermeulen, and A. Algra, “Benefits of carotid patching: a prospective randomized study with long-term follow-up.,” *Ann Vasc Surg*, vol. 8, pp. 54–58, Jan 1994.
- [7] S. I. Myers, R. J. Valentine, A. Chervu, B. L. Bowers, and G. P. Clagett, “Saphenous vein patch versus primary closure for carotid endarterectomy: long-term assessment of a randomized prospective study.,” *J Vasc Surg*, vol. 19, pp. 15–22, Jan 1994.
- [8] R. Bond, K. Rerkasem, A. R. Naylor, A. F. Aburahma, and P. M. Rothwell, “Systematic review of randomized controlled trials of patch angioplasty versus primary closure and different types of patch materials during carotid endarterectomy.,” *J Vasc Surg*, vol. 40, pp. 1126–1135, Dec 2004.
- [9] C. B. Rockman, E. A. Halm, J. J. Wang, M. R. Chassin, S. Tuhim, P. Formisano, and T. S. Riles, “Primary closure of the carotid artery is associated with poorer outcomes during carotid endarterectomy.,” *J Vasc Surg*, vol. 42, pp. 870–877, Nov 2005.
- [10] A. V. Kamenskiy, I. I. Pipinos, A. S. Desyatova, Y. E. Salkovskiy, L. Y. Kossovich, I. V. Kirillova, L. A. Bockeria, K. M. Morozov, V. O. Polyayev, T. G. Lynch, and Y. A. Dzenis, “Finite element model of the patched human carotid.,” *Vascular And Endovascular Surgery*, vol. 43, pp. 533–541, Oct 2009.
- [11] N. M. Maurits, G. E. Loots, and A. P. Veldman, “The influence of vessel wall elasticity and peripheral resistance on the carotid artery flow wave form: A cfd model compared to in vivo ultrasound measurements,” *Journal of Biomechanics*, vol. 40, pp. 427–436, 2007.
- [12] H. F. Younis, M. R. Kaazempur-Mofrad, R. C. Chan, A. G. Isasi, D. P. Hinton, A. H. Chau, L. A. Kim, and R. D. Kamm, “Hemodynamics and wall mechanics in human carotid bifurcation and its consequences for

- atherosclerosis: Investigation of inter-individual variation,” *Biomechan Model Mechanobiol*, vol. 3, pp. 17–32, 2004.
- [13] M. Tambasco and D. A. Steinman, “Path-dependent hemodynamics of the stenosed carotid bifurcation,” *Annals of Biomedical Engineering*, vol. 31, pp. 1054–1065, May 2003.
- [14] P. F. Fischer, F. Loth, S. E. Lee, S.-W. Lee, D. S. Smith, and H. S. Bassiouny, “Simulation of high-reynolds number vascular flows,” *Comput Methods Appl Mech Eng*, vol. 196, pp. 3049–3060, 2007.
- [15] S. E. Lee, S.-W. Lee, P. F. Fischer, H. S. Bassiouny, and F. Loth, “Direct numerical simulation of transitional flow in a stenosed carotid bifurcation.,” *J Biomech*, vol. 41, pp. 2551–2561, Aug 2008.
- [16] C. G. Caro, J. M. Fitz-Gerald, and R. C. Schroter, “Atheroma and arterial wall shear. observation, correlation and proposal of a shear dependent mass transfer mechanism for atherogenesis.,” *Proc R Soc Lond B Biol Sci*, vol. 177, pp. 109–159, Feb 1971.
- [17] A. M. Malek, S. L. Alper, and S. Izumo, “Hemodynamics shear stress and its role in atherosclerosis,” *JAMA*, vol. 282:21, pp. 2035–2042, 1999.
- [18] Y. S. Chatzizisis, A. U. Coskun, M. Jonas, E. R. Edelman, C. L. Feldman, and P. H. Stone, “Role of endothelial shear stress in the natural history of coronary atherosclerosis and vascular remodeling: molecular, cellular, and vascular behavior.,” *J Am Coll Cardiol*, vol. 49, pp. 2379–2393, Jun 2007.
- [19] B. I. Tropea, S. P. Schwarzacher, and A. Chang, “Reduction of aortic wall motion inhibits hypertension-mediated experimental atherosclerosis,” *Artheroscler. Thromb. Vasc. Biol.*, vol. 20, pp. 2127–2133, 2000.
- [20] A. W. Clowes, M. A. Reidy, and M. M. Clowes, “Mechanisms of stenosis after arterial injury.,” *Lab Invest*, vol. 49, pp. 208–215, Aug 1983.
- [21] B. E. Sumpio, “Hemodynamic forces and the biology of the endothelium: signal transduction pathways in endothelial cells subjected to physical forces in vitro.,” *J Vasc Surg*, vol. 13, pp. 744–746, May 1991.
- [22] B. A. Purinya and V. A. Kas’yanov, “Changes in the mechanical properties of human coronary arteries with age,” *Mechanics of Composite Materials*, vol. 13, no. 2, pp. 251–255, 1977.
- [23] G. A. Holzapfel, G. Sommer, C. T. Gasser, and P. Regitnig, “Determination of layer-specific mechanical properties of human coronary arteries with nonatherosclerotic intimal thickening and related constitutive modeling.,” *Am J Physiol Heart Circ Physiol*, vol. 289, pp. H2048–H2058, Nov 2005.
- [24] D. J. Patel and J. S. Janicki, “Static elastic properties of the left coronary circumflex artery and the common carotid artery in dogs.,” *Circulation Research*, vol. 27, pp. 149–158, Aug 1970.
- [25] T. E. Carew, R. N. Vaishnav, and D. J. Pater, “Compressibility and constitutive equation for arterial wall,” *Circulation Research*, vol. 23, pp. 61–68, 1968.
- [26] M. R. Kaazempur-Mofrad, H. F. Younis, S. Patel, A. Isasi, C. Chung, R. C. Chan, D. P. Hinton, R. T. Lee, and R. D. Kamm, “Cyclic strain in human carotid bifurcation and its potential correlation to atherogenesis: Idealized and anatomically-realistic models,” *Journal of Engineering Mathematics*, vol. 47,

- pp. 299–314, 2003.
- [27] S.-W. Lee, L. Antiga, J. D. Spence, and D. A. Steinman, “Geometry of the carotid bifurcation predicts its exposure to disturbed flow.,” *Stroke*, vol. 39, pp. 2341–2347, Aug 2008.
- [28] A. Delfino, *Analysis of stress field in a model of the human carotid bifurcation*. PhD thesis, Ecole Polytechnique Federale DeLausanne, Lausanne, 1996. No 1599.
- [29] K. S. Hunter, C. J. Lanning, S.-Y. J. Chen, Y. Zhang, R. Garg, D. D. Ivy, and R. Shandas, “Simulations of congenital septal defect closure and reactivity testing in patient-specific models of the pediatric pulmonary vasculature: A 3d numerical study with fluid-structure interaction.,” *J Biomech Eng*, vol. 128, pp. 564–572, Aug 2006.
- [30] J. E. Shigley and C. R. Mischke, *Mechanical Engineering Design*. McGraw-Hill, New York, 1989.
- [31] D. L. Fry, “Mathematical models of arterial transmural transport.,” *Am J Physiol*, vol. 248, pp. H240–H263, Feb 1985.
- [32] P. Tontonoz, L. Nagy, J. G. Alvarez, V. A. Thomazy, and R. M. Evans, “Ppargamma promotes monocyte/macrophage differentiation and uptake of oxidized ldl.,” *Cell*, vol. 93, pp. 241–252, Apr 1998.
- [33] B. S. Conklin, R. P. Vito, and C. Chen, “Effect of low shear stress on permeability and occludin expression in porcine artery endothelial cells.,” *World J Surg*, vol. 31, pp. 733–743, Apr 2007.
- [34] R. Ross, “The pathogenesis of atherosclerosis: a perspective for the 1990s.,” *Nature*, vol. 362, pp. 801–809, Apr 1993.
- [35] W. S. Moore, *Vascular Surgery: A Comprehensive Review*, ch. Extracranial Cerebrovascular Disease: the Carotid Artery, pp. 617–658. 1983.
- [36] D. Rosenthal, J. P. Archie, M. H. Avila, D. F. Bandyk, J. D. Carmichael, G. P. Clagett, J. L. Hamman, H. M. Lee, P. R. Liebman, J. L. Mills, S. L. Minken, G. W. Plonk, M. P. Posner, R. B. Smith, and S. T. String, “Secondary recurrent carotid stenosis.,” *J Vasc Surg*, vol. 24, pp. 424–8; discussion 428–9, Sep 1996.
- [37] N. A. Darvish, *Comparative Evaluation of Carotid Endarterectomy Results In Relation To Angioplasty Techniques (Rus: Сравнительная оценка результатов каротидной эндартэктомии в зависимости от методов пластики)*. PhD thesis, Bakoulev Scientific Center for Cardiovascular Surgery, M., 2002.